Engineering Structures 187 (2019) 43–56

Contents lists available at ScienceDirect

Engineering Structures

journal homepage: www.elsevier.com/locate/engstruct

Quasi-static cyclic testing and analytical investigation of steel plate shear walls with different post-tensioned beam-to-column rocking connections

Daniel M. Dowden[a,*], Michel Bruneau[b]

[a] Department of Civil and Environmental Engineering, Michigan Technological University, Houghton, MI 49931, United States
[b] Department of Civil, Structural, and Environmental Engineering, University at Buffalo, Buffalo, NY 14260, United States

ARTICLE INFO

Keywords:
Self-centering
Steel plate shear wall
Moment frame
Rocking connection
Seismic response
Resilient structure
Seismic performance

ABSTRACT

Self-Centering Steel Plate Shear Walls (SC-SPSW) have been recently proposed to help achieve possible immediate occupancy following an earthquake for buildings located in regions of high seismicity. For this purpose, like other recently developed low-damage systems, SC-SPSWs seek to: (1) eliminate damage to the surrounding gravity frame of the seismic force resisting system; (2) provide frame recentering, in order to return the building back to its pre-earthquake near vertical alignment, and; (3) concentrate hysteretic energy to replaceable elements, providing rapid and practical reparability.

A testing program was conducted investigating the quasi-static cyclic behavior of SC-SPSW systems detailed with three different beam-to-column connections and two SPSW infill configurations. Specimens consisted of one-third scaled single-bay three-story frames. Results are presented for SC-SPSWs detailed with three different post-tensioned (PT) beam-to-column rocking connections that: either (1) rock about the top and bottom beam flanges; (2) rock about the top beam flanges only referred to as the NewZ-BREAKSS connection, or; (3) rock about the beam centerline. The latter two connections were investigated to mitigate floor system damage due to PT boundary frame expansion (i.e., beam-growth) that occurs with the first mentioned rocking connection detail. Experimental and numerical results are presented for both a solid infill web plate and infill web strip configuration. Results presented show that solid infill web plates provide some additional strength and energy dissipation due to their strength in compression and affects frame recentering for quasi-static loading conditions of progressive increasing displacement cycles. In contrast, infill web strips are essentially tension-only and have the benefit that they are not susceptible to tearing from the boundary frame and does not affect frame recentering. Numerical results show that the compression strength of the solid infill web plate in these experiments was approximately 10 percent that of the yield strength of the infill web plates in tension. Furthermore, lessons learned from this testing program are presented that show that for a multiple actuator configuration along the height of a multi-story SPSW specimen, a top level displacement control with force control of the lower actuators is necessary to avoid undesired actuator interaction along the frame heights.

1. Introduction

A Self-Centering Steel Plate Shear Wall (SC-SPSW) is a robust and ductile Seismic-Force Resisting System (SFRS) intended to provide rapid reparability after a design level earthquake for buildings located in regions of high seismicity [1,2]. It combines the high energy dissipation benefits of conventional steel plate shear wall infill web plates [3–5] together with a self-centering capability that is achieved through the use of post-tensioned (PT) beam-to-column rocking joint connections. For the purpose of defining what constitutes a recentered system, here a frame is considered to be recentered if its residual interstory drift ratio is 0.2 percent or less. This is equal to the typical maximum out-of-plumb tolerance of new construction and represents a condition where no structural realignment is necessary for structural stability. Unlike conventional SFRSs where cumulative inelastic deformations could lead to significant residual drifts and hysteretic energy dissipation in the frame's beam and column components lead to components that are not easy to repair/replace after they have yielded, the proposed SC-SPSW limits energy dissipation to more easily replaceable infill web plates.

This paper presents quasi-static cyclic tests of one-third scale single-bay three-story specimens that were conducted as part of a larger experimental program to investigate the system performance of SC-SPSWs [6–8]. The SC-SPSWs investigated reported here were detailed with three different post-tensioned (PT) beam-to-column rocking joint

* Corresponding author.
E-mail address: dmdowden@mtu.edu (D.M. Dowden).

https://doi.org/10.1016/j.engstruct.2019.02.048
Received 6 November 2018; Received in revised form 10 February 2019; Accepted 20 February 2019
Available online 28 February 2019

connections and two different web plate configurations, namely: solid infill web plates and infill web strips. The latter infill web strip configuration was initially conceived to compare the response of SPSWs with a case where the angle of inclination of the tension field is controlled. However, beyond that as presented subsequently, the use of infill web strips provides some potential advantages over solid infill web plates as a possible alternative worthy of consideration. Tests were also conducted to obtain the response of the SC-SPSW specimens without their infill web plates/strips for comparisons. SC-SPSWs with the three different types of connections investigated are designated as the Flange Rocking (FR), NewZ-BREAKSS (NZ), and Centerline Rocking (CR) frame, namely frames with beam-to-column rocking connections that: (1) rock about the top and bottom beam flanges, (2) only rock about the top beam flanges also referred to as a NewZ-BREAKSS connection [9] and; (3) rock about the beam centerline, respectively. The latter two beam-to-column rocking connections were investigated as methods to eliminate floor/roof diaphragm damage due to PT boundary frame expansion (a.k.a., beam-growth) that typically occurs with FR connections [10–15]. Furthermore, the following nomenclature is used subsequently to differentiate each test specimen, where the following acronyms are appended to the "frame type" (i.e., FR, NZ, CR): W = solid infill web plate, B = no infill web plate (also referred to as the PT boundary frame, or the bare frame condition), and S = infill web strips. For example, FRW is a flange-rocking frame with solid infill web plate, NZB is a NewZ-BREAKSS frame with no infill web plate/strips, and CRS is a centerline rocking frame with infill web strips.

2. Overview of self-centering steel plate shear walls

The hysteretic energy dissipation mechanism of a SC-SPSW is achieved through elastic shear buckling of the infill web plate and yielding of the infill web plate through diagonal tension field action. The surrounding beams (horizontal boundary elements or HBEs), columns (vertical boundary elements or VBEs), and PT beam-to-column (HBE-to-VBE) rocking joints, comprising the PT boundary frame are designed to remain essentially elastic. Furthermore, to facilitate a near damage free PT boundary frame, the base connections of the SC-SPSW columns should be detailed to allow free rotation without the formation of a plastic hinge. One such detail is presented in this paper; an alternative VBE base connection in SC-SPSWs was investigated elsewhere [7]. Note that the testing program presented investigates in-plane loading effects only. In consideration of bi-directional effects, the pinned based column detail might need to be detailed to accommodate out-of-plane rotation if calculated base rotation demands in that direction showed this to be necessary. It is also noted that for replacement of the infill webs following a design level earthquake, one possible approach of replacement consists of pushing the buckled infill web plates out-of-plane in the same direction away from the original plane and welding the infill web plate replacement on the opposite side of the steel beam flange connection tab plate (i.e., steel fish plate) before removing the damaged one. That sequence would provide some level of wall strength during replacement in case aftershocks are of concern.

The yield mechanism of the infill web plate is identical in all SPSW frames (i.e. conventional and self-centering SPSWs). The differences in global seismic response arise due to the kinematics and hysteretic response of the steel boundary frame HBE-to-VBE connections. Accordingly, Fig. 1 presents the basic kinematic response for a rightward drift at an intermediate level of a single-bay multi-story SC-SPSW frame for each of the three different rocking connections investigated, where: P_s is the post-tension axial force applied on the HBE associated with a HBE-to-VBE joint connection for the FR frame, and P_{s1} and P_{s2} is the post-tension axial compression force applied on the HBE at the gap-opening and gap-closing locations of the HBEs for frame NZ and CR, respectively. Note that the beam to column bolted shear plates are not shown in Fig. 1 for clarity. It is important to point out that the shear plate bolted connections need to be detailed to accommodate rotation of the joint as shown in the figure. In the testing program reported here, this was achieved through the use of long-slotted-horizontal holes for frames FR and NZ shear plate bolts. For frame CR a true pin connection was used.

In particular, for frame NZ and CR, the post-tension elements need to be anchored to the HBE and cannot be continuous across the length of the HBE (as done for the FR frame). This is required in order to obtain the drift induced elastic PT elongations needed for recentering. Additionally, while the PT elements at the gap-opening locations will always contribute to frame recentering, the PT elements at the gap-closing locations may or may not, depending on the relationship between the initial PT force provided, P_o, and the relative joint rotation due to frame drift. Note that the location of the PT anchor point along the HBE will affect the strain demands of the PT elements at the maximum target drift, and should be located along the HBE to ensure that the PT strains remain elastic up to that drift demand. Further differences in frame response for the different joint connections will be highlighted subsequently through nonlinear pushover analyses after the numerical modeling is presented.

3. Prototype building and model specimen design

The prototype building used for this project was based on the 3-story building used in the SAC Steel Project [16]. Originally developed as a benchmark building for steel moment frame systems, the SAC buildings have been used extensively as a benchmark building by researchers for other SFRSs including SC-SPSWs and conventional SPSWs [2,17]. The 3-story SAC building is representative of a standard office building with structural steel framing construction located in Los Angeles, California, situated on stiff soil (Site Class *D* per ASCE 7-10 [18] definition), and assumed to have a total of six lateral force resisting frames in each primary orthogonal building direction. The 10% in 50 year seismic hazard level, short-period (i.e., S_{DS}) and 1 s-period (i.e., S_{D1}) spectral response acceleration parameters for the design level earthquake, based on the 2009 NEHRP seismic hazard maps for 5% equivalent viscous damping, were obtained to be 1.598 g and 0.842 g, respectively.

For these tests, a scale factor of three (i.e., one-third scale of the full-scale prototype) was selected for the model to facilitate testing. As an initial design step, the lateral frames for the prototype building were assumed to be conventional SPSWs and the boundary frame members were designed using the *indirect capacity design approach* per the AISC *Seismic Provisions* [19]. Furthermore, the equivalent lateral force procedure per ASCE 7-10 [18] was performed to obtain the design seismic forces using the additional parameters: R = response modification factor for SPSWs = 7; I = importance factor = 1; W = frame tributary seismic weight = (6503 kN) * (1/6 frames) = 4817 kN. The tributary design base shear for the prototype frame was then calculated to be 1103 kN with a story shear vertical distribution along the frame height of 574 kN, 925 kN, and 1103 kN at Level 3, 2, and 1 respectively. Next, using the calculated design story shears, the thickness of the infill web plates was determined assuming that the infill web plates resist 100% of the story shears at each level. For initial sizing purposes, ASTM A36 was assumed for the infill web plate material. The required thickness of the infill web plates was then calculated using the design shear strength equation according to the AISC *Seismic Provisions* [19] for SPSWs assuming an α = angle of web yielding tension field measured from the vertical of 45 deg.

Next, a monotonic nonlinear pushover analysis using a strip model [3] was performed for the SC-SPSW model frames, using the geometrically scaled boundary frame and infill web plate member sizes obtained from the preliminary prototype SPSW design. The infill web strips were assigned elastic-perfectly plastic nonlinear axial hinges. The mechanical properties of the boundary frame and PT members were ASTM A992 and ASTM A416, respectively, and designed to remain elastic up to 4% roof drift. Finally, the numerical models were checked

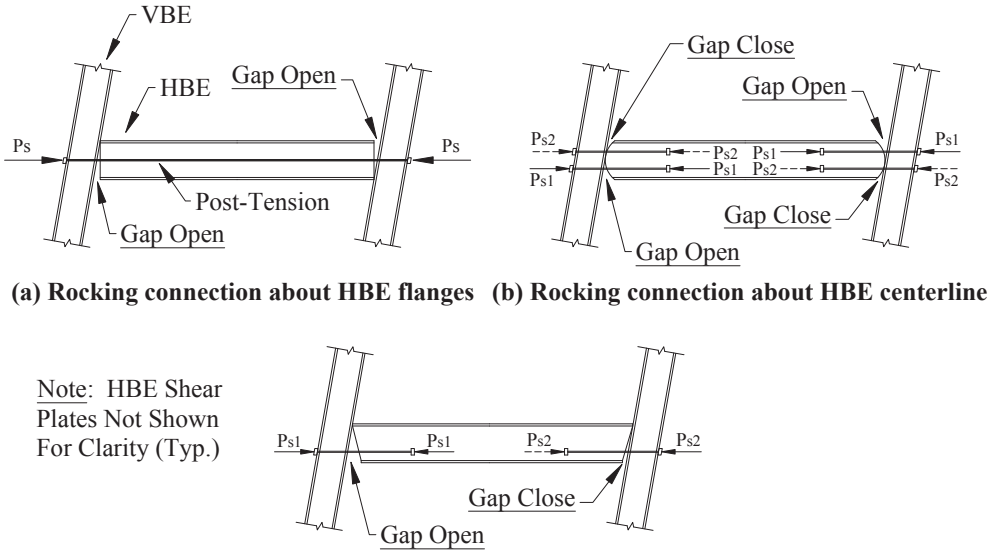

Fig. 1. Rocking mechanisms (for rightward drift).

using material coupons representative of the infill web plates to be used in the experimental testing phase.

4. Numerical modeling

Numerical models of the SC-SPSW frames were developed using the program OpenSees [20]. The boundary frame members, infill web plates, and post-tension materials were ASTM A992, A1008, and A416, respectively. The strip model approach noted above was used to model the SPSW infill web plate. Accordingly, the infill web plate was modeled using a series of truss elements, where each truss element was assigned an axially yielding member model using the *Hysteretic Material* definition to account for non-linear hysteretic behavior. In particular, the material definition has a user option of a "*pinchx*" and "*pinchy*" factor that provides pinching for strain and stress during reloading, respectively. To model tension-only of the infill web plates, values of 1.0 and 0.0001 was used for those factors, respectively. Furthermore, for calibration of experimental results (presented subsequently), both a tension-only (TO) and a simplified combined tension–compression (TC) hysteretic model for the infill web strips was considered, where the TC model considers some compression strength contribution of the solid infill web plate. To facilitate the latter, the *Elastic-Perfectly Plastic* and *Hysteretic Material* definitions were combined using the *Parallel Material* definition offered by OpenSees. For this purpose, the *Hysteretic Material* component is identical to that used in the TO model and the *Elastic-Perfectly Plastic* component is modeled as compression-only behavior. This simplified TC model approach was proposed in [8] where a more detailed presentation on the TC model is provided. The backbone of the uniaxial tension stress-strain mechanical properties used in the numerical models is shown in Fig. 2. Material coupon tension tests for the boundary frame members and PT strands were not performed as it was expected that these components would remain essentially elastic.

The PT elements were modeled using truss elements. The yield strength of the PT elements was assumed to be 90% of the ultimate tensile strength of the PT material (F_{pu} = 1.9 GPa) and the elastic modulus was assumed to be 200 GPa. For frame FR, these elements were modeled with the *Steel02 Material Giuffre-Menegotto-Pinto Material* definition with a strain hardening ratio of 0.02. To simulate the initial applied PT force, the user option of providing an initial stress value was used. For frame NZ and CR, the PT elements used the *Elastic-Perfectly Plastic Gap Material* definition with no strain hardening, which allows for tension-only behavior. Recall that for these connections, PT elements at the closing joint locations will relax. This latter material

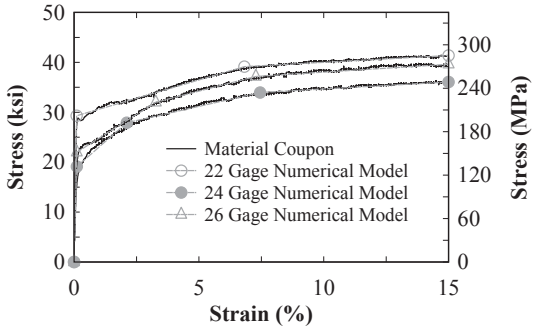

Fig. 2. Infill web plate coupons.

definition simulates that behavior, which also allows a user input of an initial negative strain to simulate the initial applied PT forces. Additionally, the PT elements were designed to remain elastic up to a target 4% roof drift. Therefore, for this purpose, an elastic-perfectly plastic material definition for the PT elements was deemed acceptable. Furthermore, the rocking connection was modeled using compression-only springs (using the *Elastic-No Tension Material* definition) at the HBE-to-VBE contact flange locations in combination with the use of nodal constraints and *rigidlink beams*. An elevation of the numerical strip model for frame FR is presented in Fig. 3 (frame NZ and CR similar). Additional modeling of connection details in OpenSees for the typical HBE-to-VBE joints is presented in Fig. 4. In that figure, joint constraints in the vertical degree-of-freedom were used at nodes 1 and 2 where noted, to transfer beam shear forces to the column.

5. Numerical frame response general comparison

To provide some insight on general characteristics in behavior between SC-SPSWs detailed with the different beam-to-column rocking connections, monotonic pushover curves are presented in Fig. 5 using the designed test specimen parameters (to be presented subsequently). Furthermore, this investigation is only made for the PT boundary frame, with the understanding that the total response is a superposition of the effects of the PT boundary frame and the infill web plate. From Fig. 5, the following general observations are supported:

(1) Frame FRB has a bilinear response, with two linear frame stiffnesses, K1 and K2. Frame stiffness K1 occurs when the HBE-to-VBE

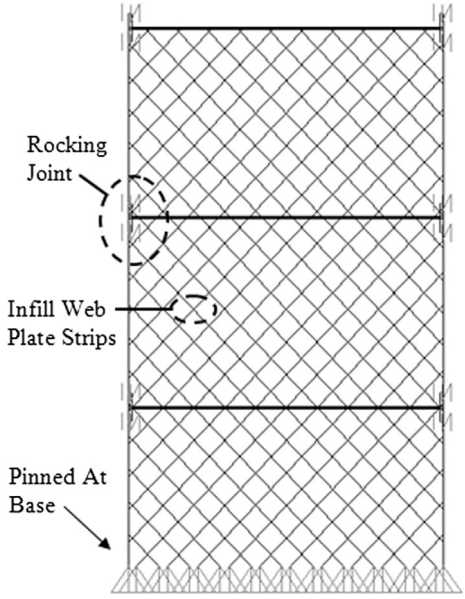

Fig. 3. Frame FR numerical model.

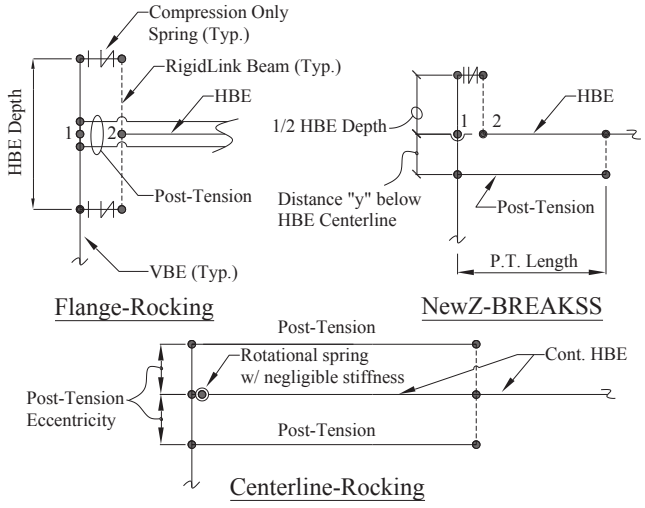

Fig. 4. OpenSees: rocking joints.

joints are in full contact and compressed together by the initial PT force, P_o. Upon lateral frame loading, the axial force clamping effects of P_o at the HBE-to-VBE connection decreases as a result of decompression of the HBE-to-VBE joints during frame drift. Frame stiffness K2 occurs when the HBE-to-VBE joint just opens when the PT tensile pre-strain at corresponding P_o has been exceeded. At this condition, the presence of PT force P_o and a lever arm from the PT centroid to the HBE-to-VBE rocking point generates a moment, commonly referred to as the "decompression moment". From the point of decompression moment, all subsequent PT force demands are from a combination of $P_o + \Delta P$ where ΔP is the additional tension force in the PT due to strand elongation during gap opening from increased frame drift.

(2) Frame NZB is also bilinear, but for different kinematics than for frame FRB, leading to the different frame stiffnesses, K3 and K4. The frame has a stiffness of K3 when all PT elements are in tension. Should the PT elements at the closing-joints become fully relaxed (see Fig. 1c), the frame will then have a reduced frame stiffness K4.

(3) Frame CRB also has a bilinear response with different frame stiffnesses K5 and K6, developing for same reasons as frame NZB. Furthermore, if the eccentricity to the centroid of the PT elements

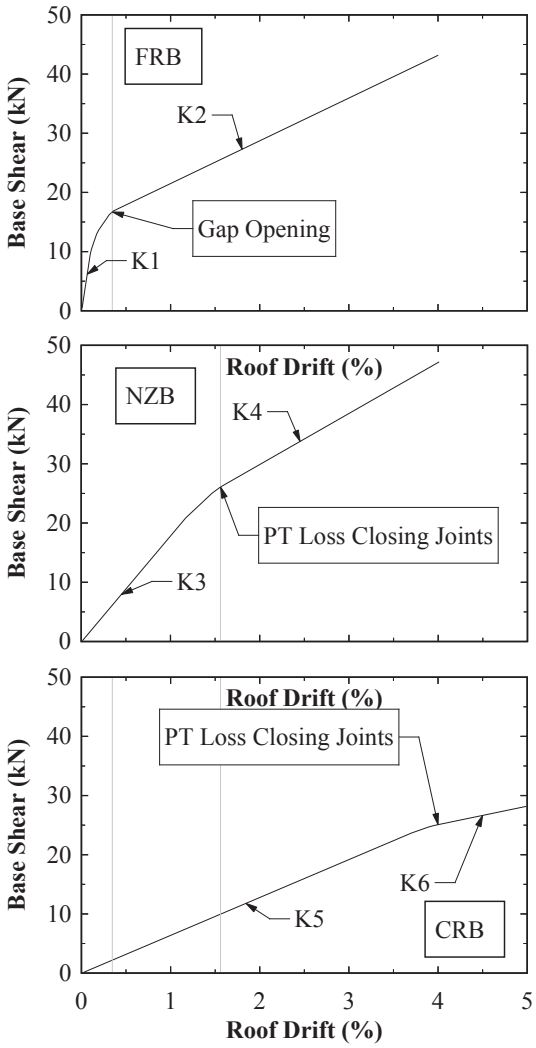

Fig. 5. PT boundary frame - Monotonic pushover comparison.

to the HBE-to-VBE rocking point and the initial PT forces are identical to frame NZB, frame CRB will have a larger stiffness than frame NZB (i.e., K5 > K3 and K6 > K4) for the reason that frame CRB has both an opening and closing joint at each HBE-to-VBE joint, contrary to frame NZB (see Fig. 1b).

Note that for the frame FRB and NZB curves presented, the quantity of PT strands, PT eccentricity from the rocking point, and initial PT force provided are identical. Yet, it is observed in Fig. 5 that the initial stiffness of frame FRB is larger (i.e., K1 > K3). This is due to the presence of the decompression moment effects inherent with frame FRB. Also note that, with respect to the secondary stiffness, frame NZB is stiffer (i.e., K4 > K2) due to the fact that the PT strands on frame NZB are shorter. In general, the larger initial frame stiffness will be more efficient for frame recentering response [6]. For this reason, frame FRB provides the most efficient recentering response of the three different connections investigated as a result of its larger initial stiffness provided by the decompression moment (but at the expense of beam-growth).

6. Test specimen, setup, and loading protocol

The final specimen design showing the solid infill web plate and infill web strip configurations is presented in Fig. 6 for frame FR and CR, respectively (frame NZ similar). The second floor beam section is

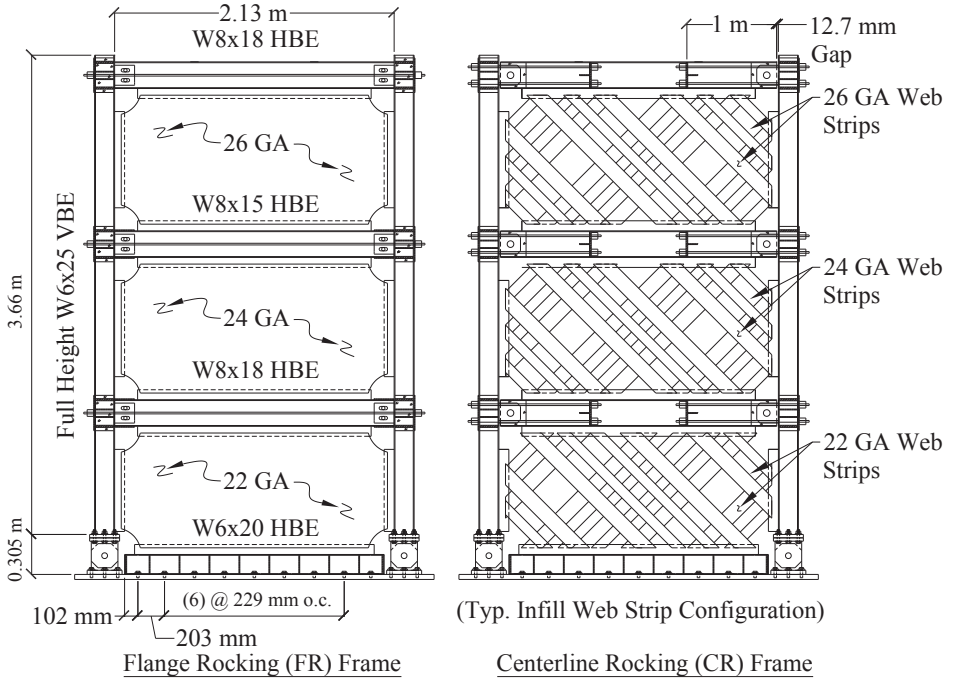

Fig. 6. Test frame elevations.

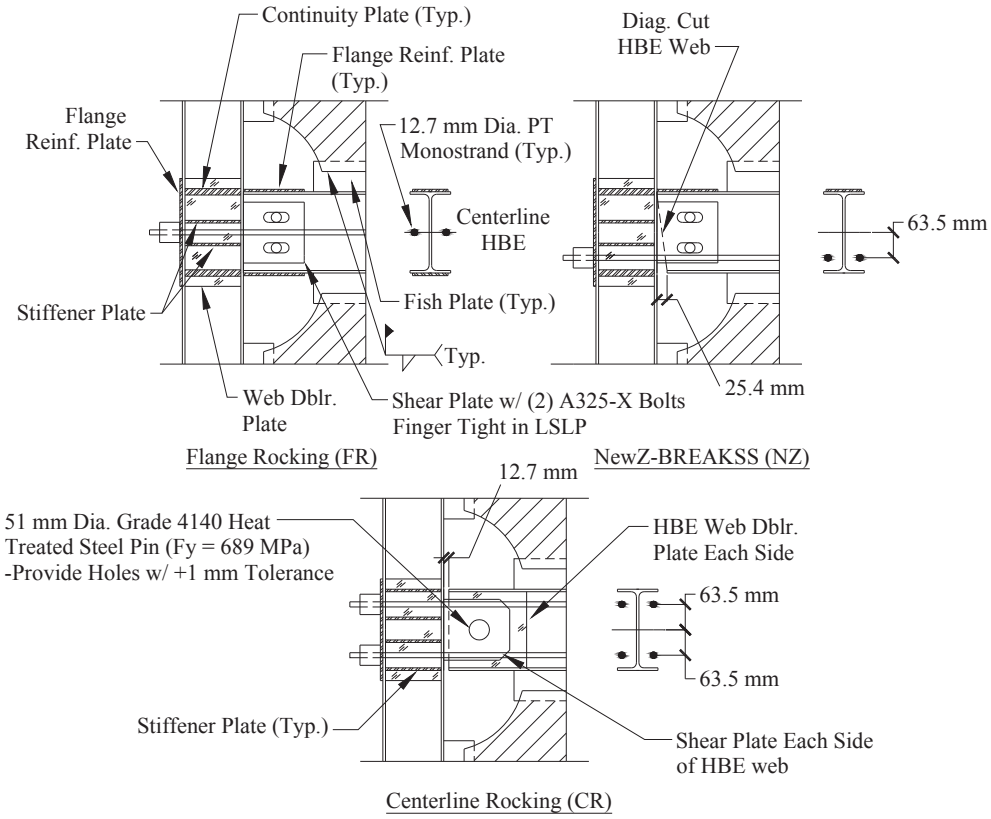

Fig. 7. HBE-to-VBE joint details.

lighter than the roof beam because the demands on that beam due to yielding of the infill web plate are not as large as those developed at the roof. The roof beam in flexure and shear must resist the vertical component of the yielded 26 GA infill web plate, whereas the second floor level beam only resists the difference between the vertical components of the yielded 24 GA and 26 GA infill web plates. The connection detail for each of the three different frame types (i.e., FR, CR, and NZ) are shown in Fig. 7. Note that although the actual test specimen detail for frame CR is different than that shown in Fig. 1b presented earlier, the pinned connection detail behavior is identical. At the foundation level, a clevis and pin connection was provided at the VBE base to allow free rotation without the formation of a plastic hinge. An anchor beam

bolted to the foundation plate was provided to transfer the infill web plate forces to the laboratory strong-floor. Furthermore, an initial post-tensioning force, P_o, of approximately 20% of the PT yield strength was targeted for frame FR and NZ, where the PT yield strength, F_{yPT}, was assumed to be 90% of the ultimate tensile strength, F_{uPT}, of the PT strands. For frame CR, 30% of F_{yPT} was targeted. This larger initial PT force for frame CR is a reflection of the smaller eccentricity of the PT from the rocking point, compared to the other frames as shown in Fig. 7. Note that the selection of the initial force P_o is dependent on a target PT elastic response up to a target roof drift (or interstory drift) selected by the design engineer. In the design specimens presented here, P_o was selected to target an elastic PT response up to a roof drift of 4% as noted earlier.

The test setup used an existing modular lateral bracing system developed at University at Buffalo for the experimental testing of scaled specimens [21]. The modular bracing system, hereafter referred to as the Gravity Mass Frame (GMF) system, is a self-contained structure that can support its own gravity weight, has lateral stiffness and stability in its primary transverse direction, but has insignificant lateral stiffness in its longitudinal direction. The system has a set of floor/roof diaphragms consisting of 89 mm thick steel plates with an approximate weight of 37.8 kN per plate, each supported by four S3 × 5.7 columns. Transverse lateral stiffness of the system is provided by L1.5 × 1.5 × 1/4 X-bracing connected to each pair of gravity columns at each floor plate. A total of three MTS 244.51 actuators were used for lateral loading, one located at each diaphragm level attached to the steel diaphragm plates with a built-up steel beam connection at each level with pretensioned slip-critical bolts. The test setup is shown in Fig. 8. Additional information on the test setup and instrumentation is provided in [6].

The cyclic loading protocol used to conduct the quasi-static tests was adapted from the ATC 24 [22] loading procedure and based on displacement control of the roof level actuator. Initial cycles were based on roof displacements consisting of multiples of the effective yield displacement (i.e., $1\delta_y$, $2\delta_y$, etc.), where δ_y for each specimen was obtained from nonlinear pushover analysis for each frame. After the displacement step of $4\delta_y$, the top level actuator displacement control changed to a target roof drift displacement (i.e., 2%, 2.5%, etc.). For brevity, the loading protocol history for each test specimen is not provided here but can be found in [6].

7. Lessons learned on quasi-static testing of multistory SPSWs

The first three tests were conducted on frame FR, using a displacement control scheme for all three actuator levels, with the top level actuator set to provide a “master” displacement to which displacement of the other actuators were “slaved” to be equal to a set fraction of the master displacement. The displacement shape used was based on an approximate first mode shape pattern normalized by the top story level. However, during the test, it was found that the use of this displacement control scheme lead to undesired actuator interaction across the story heights. In particular, at times, the forces applied by the actuators were acting in opposite directions and “fighting” each other to maintain the enforced lateral displacement shape at each floor level. As a consequence, the global base shear versus roof drift response of the test specimens presented in Fig. 9 exhibited a negative stiffness, suggesting global instability. Also superimposed on the plots is the results from the frame FRB test for reference. Further tests were conducted on frame FRB to explain this unexpected response. It was determined that the negative stiffness observed for frame FR was a consequence of the displacement shape imposed to the specimen using the aforementioned actuator displacement control scheme, which led to the undesirable actuator interaction observed across the stories. As shown in Fig. 10, this artifact disappeared when a combined force-and-displacement actuator control method was used for frame loading. This was done by enforcing an actuator displacement control at Level 3 and corresponding slaved actuator force control at Level 1 and 2 (with the actuator force at Level 3 being the master).

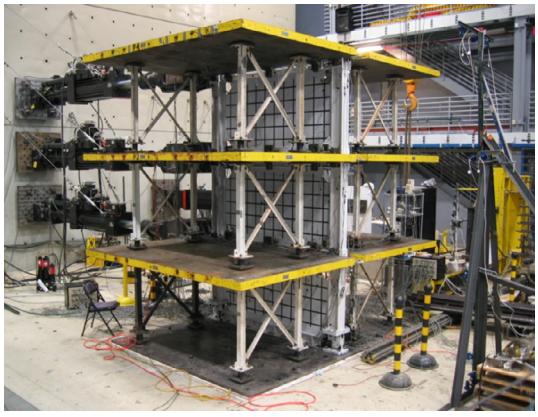

Fig. 8. Quasi-static test setup.

To provide additional insight on the displaced shape using this revised actuator control, Fig. 11 provides the displacement at each level normalized by the corresponding roof displacement for a peak positive drift cycle as indicated in the figure. The peak drifts were selected based on an elastic response and an inelastic response at the maximum positive roof drift cycle for the frames with infill web plates/strips. In Fig. 11c, an additional intermediate drift cycle is provided for reference since frames NZS and CRS were tested to larger roof drifts. It is observed that the revised actuator control lead to a reasonable approximation of the fundamental mode given by the actuator force load distribution. The noticeable difference observed for the 3 percent roof drift observed in Fig. 11a for frame NZW is due to the tearing of the infill web plate from the boundary frame in combination with the actuators at levels 1 and 2 in force control.

Note that the modified actuator control approach described above must be combined with closely monitored safety protocols to prevent uncontrolled displacements at the actuator force control levels as specimen strength degradation occurs during the tests. For the remaining frame NZ and CR tests, this alternative actuator control was used with an approximate actuator force load pattern distribution of 1, 0.66, and 0.32 at Level 3, 2, and 1, respectively; based on the approximate first mode distribution of story forces calculated per ASCE 07-10 [18]. For reasons just presented, only experimental results for frame NZ and CR are presented subsequently.

8. Experimental and numerical base shear versus roof drift response

For frame NZ and CR, each frame type was tested sequentially with a solid infill web plate (“W”), no infill web plate or PT boundary frame (“B”), and an infill web strip (“S”) configuration as described earlier. For this purpose, each test frame was left in place and only the infill web plate configuration was modified for the subsequent test.

The global response in terms of base shear versus roof drift for frame NZ and CR is presented in Fig. 12. Also included in that figure are the numerical results obtained using OpenSees and will be addressed at the end of this section. Fig. 12 and documented visual assessment support the following observations:

(1) For the infill web plate configuration in Fig. 12a, the base shear is not zero at the location of zero-drift; consequently, there is a residual drift at the zero-base shear condition, indicating that the frame is not fully recentering; similar observations were also made in [8,23]. The residual base shear is due to the development of some compression strength of the infill web plate from the random folding of the infill web plate as it is pushed through the zero drift point, after cycles of progressive drift increase. Other researchers

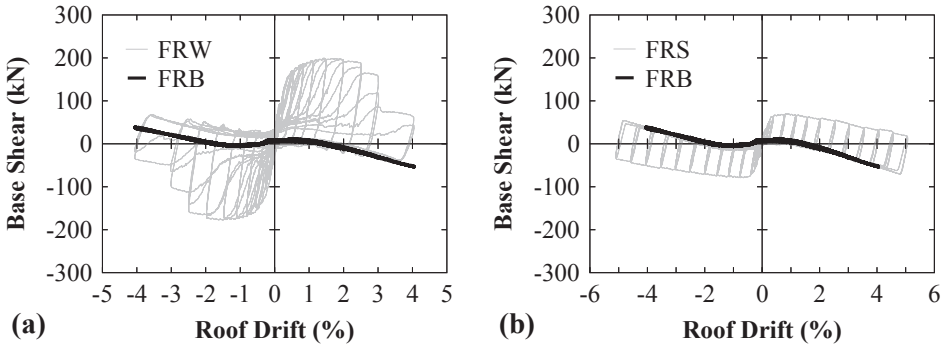

Fig. 9. Frame FR base shear versus roof drift: (a) solid infill web; (b) infill strips.

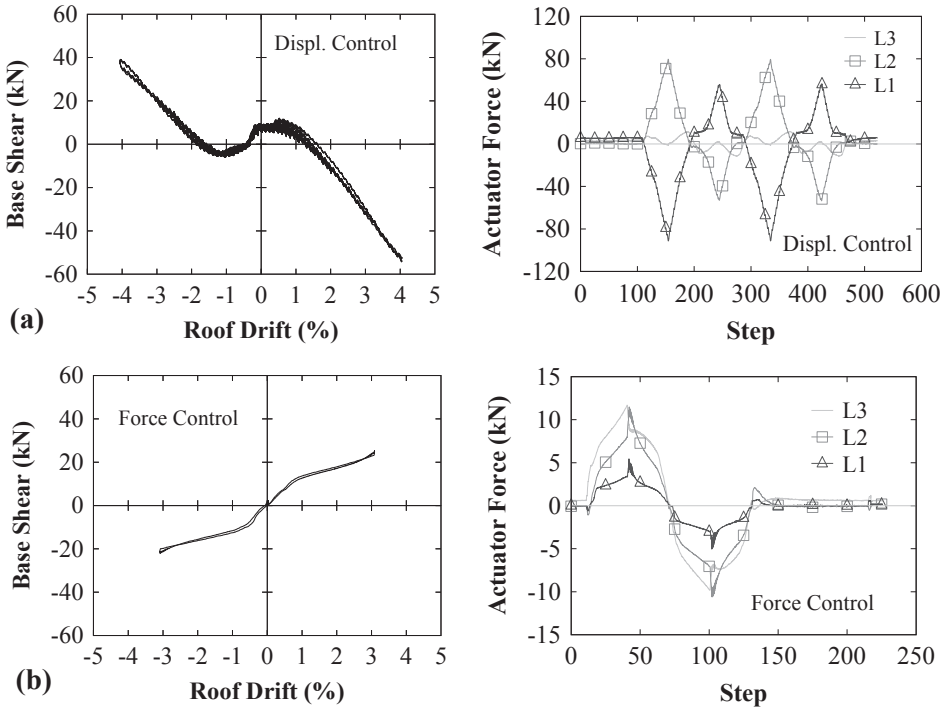

Fig. 10. FRB test: (a) displacement control; (b) force control.

reported this was due to the plastic contraction of the web plate in the direction perpendicular to the tension field direction [24]. Accordingly, the solid infill web plate configuration offers some additional energy dissipation as evidenced by the fuller hysteretic loops compared to a "flag-shaped" response that is characteristic of self-centering systems. As a consequence, the developed compression strength of the solid infill web plates, does provide some resistance against frame recentering. Based on the residual drifts shown in Fig. 12a, where residual drifts are observed to exceed 0.5 percent drift, realignment of the structural frame would be required after the earthquake [25]. Note that the influence of the developed compression strength of the infill web plate on the frame recentering response for the loading protocol used was not fully understood in the design of the test specimens. This will be addressed in a later section of this paper. However, this phenomenon is limited to quasi-static loading conditions of increasing displacement cycles. Pseudo-dynamic and shake-table tests show that the compression strength of the infill web plate does not affect frame recentering [7,26].

(2) For the PT boundary frame-only configuration in Fig. 12b, it is observed that some energy dissipation occurs as the experimental results are not completely linear elastic. Given that no infill web plates/strips are present and the PT boundary frames remained elastic for these tests, the hysteretic loops developed are attributed to friction inherent in the test setup and specimen connections. Furthermore, in comparison with frame NZW and CRW, the PT boundary frame contribution to the total base shear strength is approximately 10–15% of that for the frames having a solid infill web plate condition. Accordingly, in an SC-SPSW system, the strength and energy dissipation is essentially provided by the infill web plates only. Therefore, as was done in this test program, the infill web plates should be designed to resist 100% of the design seismic shears in an SC-SPSW system.

(3) For the infill web strip configuration in Fig. 12c, recentering is nearly perfectly achieved. That is at the zero-base shear condition, a corresponding near zero-drift condition occurs. This indicates that the infill web strips behave as ideal tension-only elements. The observation that the infill strips are tension-only, support the observation above that the larger hysteric shape at the near zero-drift location is due to the compression strength of a solid infill web plate. Furthermore, not readily apparent from the experimental curves for frame NZS, the PT elements at the Level 1 beam yielded at approximately the 4% roof drift cycle. Given that this frame was tested up to 6% roof drift provides some evidence that some PT

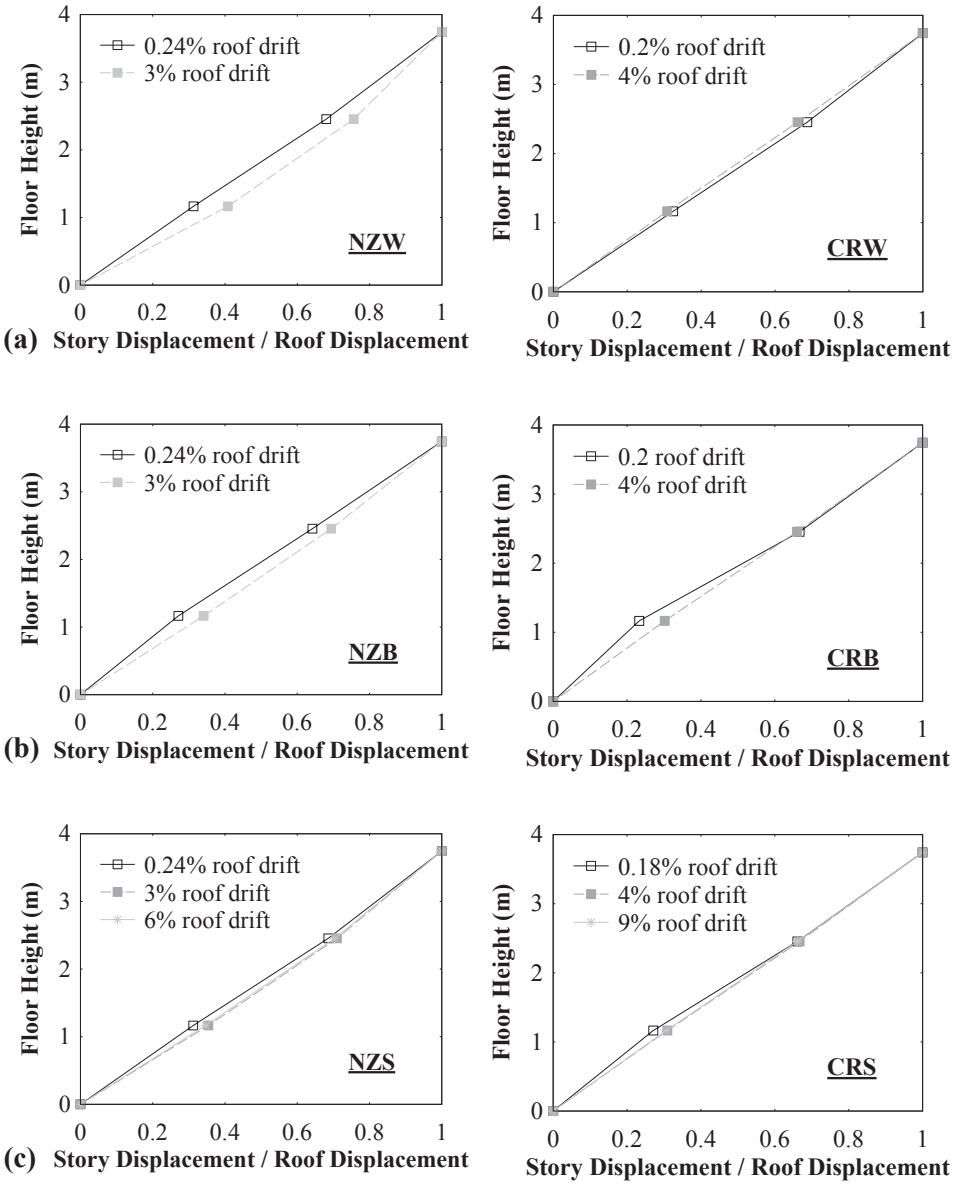

Fig. 11. Frame deflected shape: (a) solid infill web; (b) PT boundary frame; (c) infill strips.

yielding can occur without significant detrimental effects to the global frame response. That is for these tests, the PT elements at the remaining levels above was adequate to provide frame recentering. Note that the base shear strength of frames NZS and CRS are approximately 50% of the corresponding frame NZW and CRW. This is because the infill web strips were selected to be of the same thickness as the solid infill web plate condition, and gaps were left between the strips.

(4) From Fig. 12a, it can be observed that strength degradation of frame NZW and CRW initiated at approximately 2% roof drift. This was due to tearing of the infill web plate from the boundary frame (propagating from the corners of the infill web plates). In contrast, no tearing of the infill web strips occurred for frames NZS and CRS which were tested upwards to roof drifts of 6% and 9%, respectively. This was confirmed through visual observation and by observation that no strength degradation occurs in Fig. 12c. This suggests that infill web strips are not susceptible to tearing at the welded connection to the PT boundary frame compared to solid infill web plate configurations.

(5) To provide further insight on the behavior of infill web plates versus infill web strips, the hysteretic response for frame NZW and NZS is compared in Fig. 13a and b, respectively, for two consecutive displacement steps. It is observed that the hysteretic loops overlap for frame NZW. In contrast, for frame NZS, consecutive loops occur adjacent to one another with negligible overlap. Specifically, this shows that energy dissipation for the infill web strips only occurs at subsequent drifts that exceed the previous cycle, characteristic of tension-only behavior. For further clarity, Fig. 13c and d, only shows the results at a single displacement step (i.e., 2% and 6% drift for frame NZW and NZS, respectively), which show the effects at repeated displacement steps. The results show that infill web plates do provide some energy dissipation during repeated cycles attributed to the infill web plate compression contribution presented above. In contrast, the infill web strips provide no observable energy dissipation during repeated cycles. Typical infill web plate and infill web strip deformation before and after testing are shown in Fig. 14. In Fig. 14d, the tension-only behavior of the infill web strips is evident by the deformed shaped of the strips.

Numerical results of the final calibrated OpenSees model, included

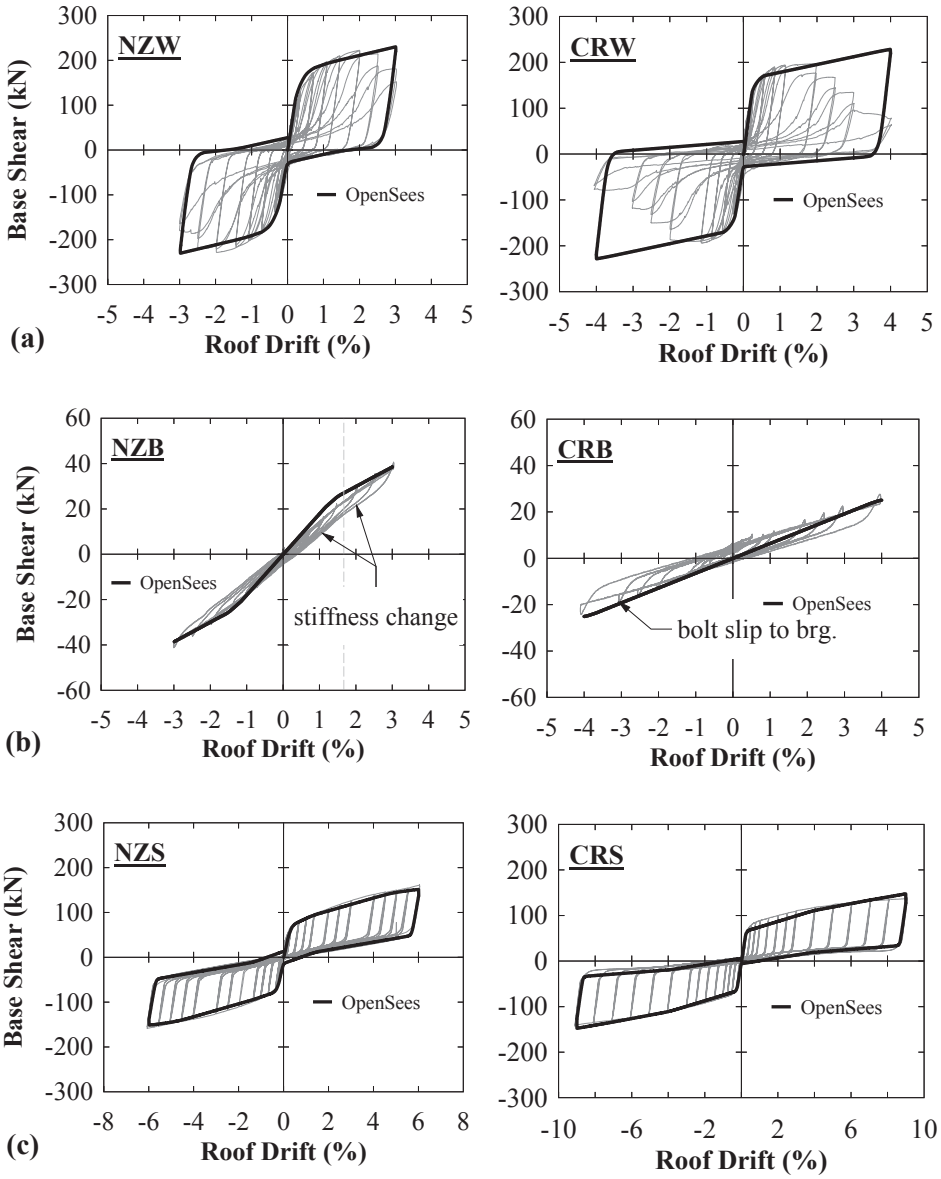

Fig. 12. Base shear versus roof drift: (a) solid infill web; (b) PT boundary frame; (c) infill strips.

in Fig. 12, are in reasonable agreement with the experimental results. As presented earlier, numerical models for frame NZW and CRW, included a combined tension–compression (TC) hysteretic model for the solid infill web plate and infill web strip. For calibration with the experiment results, approximately 20% and 10% of the yield strength of the SPSW web plates for solid infill web plates and infill web strips, respectively, were needed in the numerical model to obtain results comparable with the experimental ones. However, note that 10% of that compression value used for the infill webs actually account for the response of the PT boundary frame alone which was not entirely linear-elastic (see Fig. 12b). Recall that evidence of this was presented in Fig. 13d which shows that the infill web strips exhibit tension-only behavior. This suggests that the actual compression strength of the infill web plate for these tests is approximately 10% of the tensile yield strength of the solid infill web plate.

9. Experimental and numerical post-tension versus interstory drift response

To provide insight on the response of the PT HBE-to-VBE rocking joints, the PT response was investigated. In particular, it is the contribution of the PT clamping force and elastic elongation of the PT elements that provide global stability of the frame once the infill web plates/strips have significantly yielded. Furthermore, reporting the PT response history is insightful for frame NZ and CR, where the PT elements relax at the closing joints. Note that “relax” as used in the context of this paper, refers to a decrease in the initial post-tensioning force, P_o, as a result of a reduction in the original gap-opening position between the VBE and HBE flanges prior to lateral frame drift.

The PT force versus interstory drift response is presented in Fig. 15 for the Level 1 HBEs (results for Level 2 and 3 were similar). For frame NZ, two PT response curves are shown on a single plot representing the east and west end PT elements on the beam. For frame CR, the number of PT elements is doubled compared to frame NZ for reasons presented earlier. For brevity, only the response of the PT elements on the east end of the beam for frame CR are presented (the PT elements on the west end are similar but opposite signs). The results presented show that although an initial PT force, P_o, was provided, a reduction in PT force immediately occurs upon frame drift. This is because a HBE-to-VBE decompression moment is not present for frame NZ and CR; a distinction from frame FR where HBE-to-VBE rocking does not occur until the decompression moment has been exceeded. Furthermore, it is

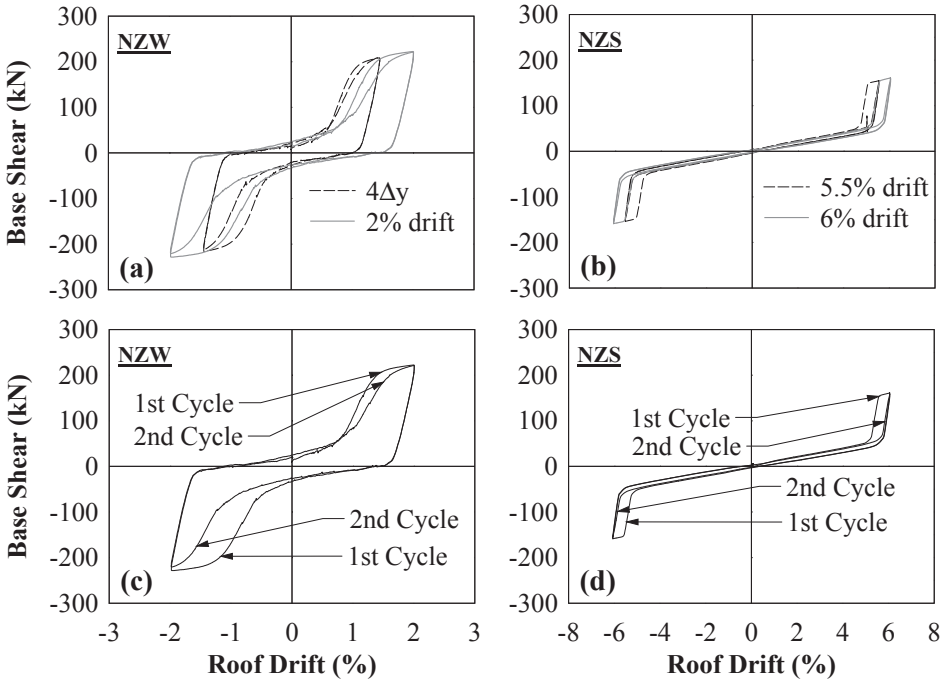

Fig. 13. Base shear vs. roof drift: (a) NZW; (b) NZS; (c) 2% drift only; (d) 6% drift only.

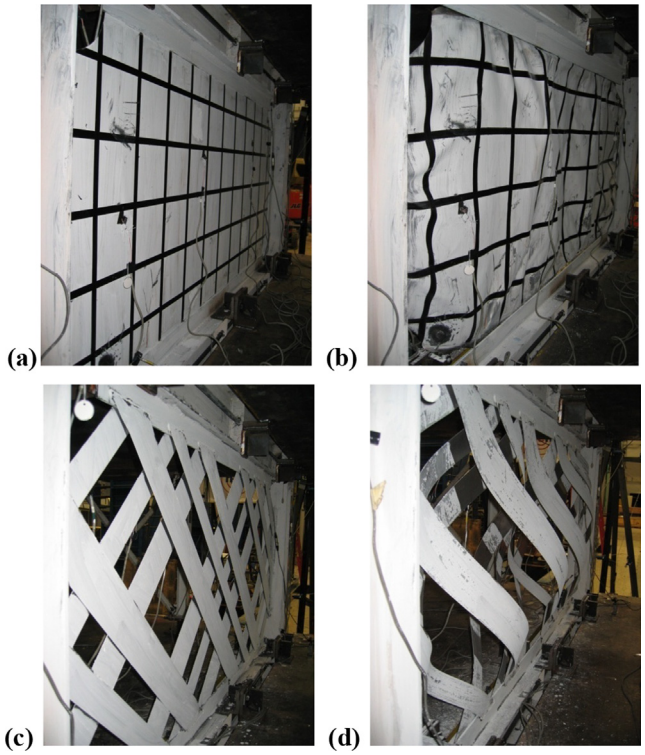

Fig. 14. Typical infill web plate/strip: (a) solid infill before test; (b) solid infill end of test; (c) infill strips before test; (d) infill strips end of test.

observed that the PT forces increase and decrease at the opening and closing HBE-to-VBE joints, respectively. In particular, at the closing joints, the PT elements are fully relaxed when the gap-closing distance exceeds the initial post-tensioning strain of the PT elements (indicated by the horizontal portions of the PT response curves). The significance of this shows that frame global stability for frame NZB and CRB is not detrimentally affected by this response. Additionally, for frame NZS and CRS, recentering is not affected by this response either (see Fig. 12c). Finally, another notable observation of the experimental response curves is that although the PT elements remained elastic during the tests (with exception of frame NZS noted earlier), there appears to be some PT hysteretic response. This is more pronounced in Fig. 15c for the frames with infill web strips. This nonlinear response is due to PT force losses in P_o between subsequent cycles and not due to hysteretic behavior. Similar observations were observed in Pseudo-dynamic and shake-table testing of SC-SPSWs [7,26].

Superimposed on the PT experimental response curves are the calculated predicted response based on analytical equations describing the PT force as a function of interstory drift. For reference, these equations are reproduced from [6] where Eqs. (1) and (2) are the PT force demands at the opening and closing joints, respectively, for frame NZ and CR.

$$P_{s1} = P_o + \left(\frac{k_{b1}k^*_{PT}}{k_{b1} + k^*_{PT}}\right)\Delta_{drift} - \frac{k^*_{PT}}{k_{b1} + k^*_{PT}}P_{HBE(VBE)} \quad (1)$$

$$P_{s2} = P_o - \left(\frac{k_{b2}k^*_{PT} + 2(k^*_{PT})^2}{k_{b2} + k^*_{PT}}\right)\Delta_{drift} - \frac{k^*_{PT}}{k_{b1} + k^*_{PT}}P_{HBE(VBE)} \quad (2)$$

In these equations, the variables are defined as follows: P_o = initial post-tension force; k_{b1} = HBE axial stiffness along length of PT at opening-joint; k_{b2} = HBE axial stiffness along length of PT at closing-joint, $k_{PT}{}^*$ = PT axial stiffness reduced by an amount proportional to the ratio of the PT force reaction at the HBE-to-VBE rocking point to that of the force in the PT elements for frame NZ (i.e., *scale factor* multiplied by k_{PT} where the *scale factor* is presented elsewhere [9] and k_{PT} is the PT axial stiffness for frame CR); Δ_{drift} = drift induced PT elongation; and $P_{HBE(VBE)}$ = horizontal reaction at the rocking point of the yield force resultant of the infill web plate acting on the VBE [3]. Additional information related to the above equations and definitions can be found in [6]. In comparison of the analytical versus experimental results, it is observed that the analytical response is conservative. That is for a given interstory drift, the analytical equations lead to larger PT force demands on the frame. Furthermore, the equations predict that the PT elements at the closing joints become fully relaxed at a smaller interstory drift than the actual condition. The conservative prediction of the equations is a reflection of the assumption of rigid boundary frame

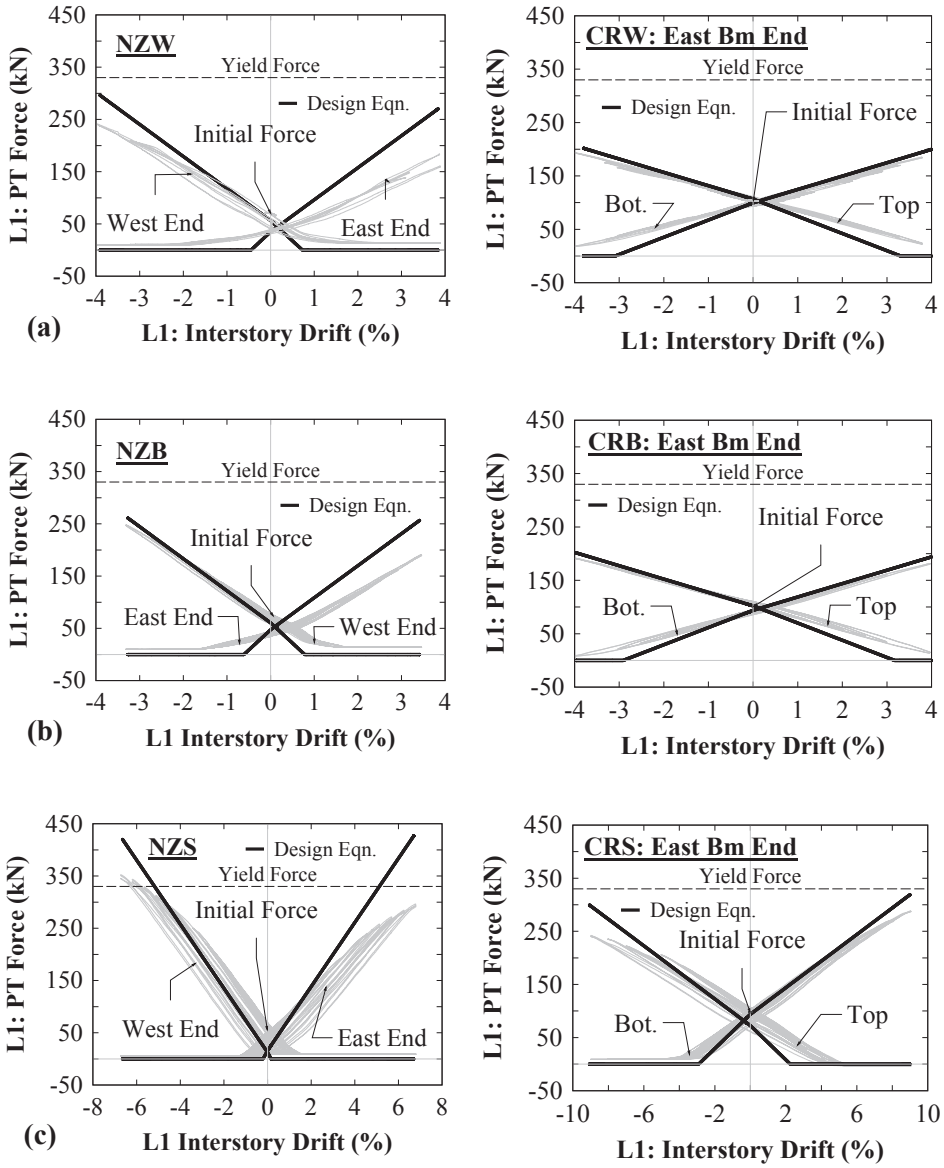

Fig. 15. PT force vs. interstory drift: (a) solid infill web; (b) PT boundary frame; (c) infill strips.

behavior assumed in the derivation of the equations presented. Also, the equations do not consider losses in P_o observed in the experimental results, due to sources such as PT anchor wedge seating. However, for the purpose of preliminary design, the equations are deemed appropriate given the modest conservatism.

10. Design calculation of HBE post-tension area

At the time of test specimen design, the effects of the solid infill web plate on recentering for quasi-static cyclic loading conditions and loading protocol used were not fully known. Although recentering was not achieved (i.e., residual roof drift of less than or equal to 0.2 percent) for the frames with this infill web plate configuration, consideration of the infill web plate effects can be incorporated into the frame design by changing the PT parameters. Accordingly, for this purpose, a simplified approach for calculation of the PT area needed to ensure a minimum target residual roof drift was developed for a particular frame configuration and presented below.

First, recall that the global force-displacement response of the PT boundary frame is bilinear elastic regardless of the rocking joint detail used. As such, the method presented here can be applied for frame types FR, NZ, and CR. However, for frame FR, subsequent equations would also need to consider diaphragm restraint effects (as a consequence of beam-growth) at the HBE-to-VBE rocking connections. One possible approach was proposed in [27]. For frame NZ and CR, diaphragm restraint is minimized as beam-growth effects are eliminated. The one exception is that for frame CR, a local slip detail would need to be accommodated at the top of the beam near the HBE-to-VBE connection where gap-opening occurs. From Fig. 12, it is realized that the compression strength of the infill web plate has the effect of vertically shifting the PT boundary frame response by an amount β, which is the assumed compression effect of the infill web plate as shown in Fig. 16a for a positive monotonic pushover drift condition. Correspondingly, the residual drift then occurs at some point λ, as shown in that figure. It then follows that, for a given β, the design effective frame stiffness K1 can be obtained for a target residual drift λ, as shown in Fig. 16b, where the effective frame stiffness is calculated by Eq. (3). The approximate PT area at each joint can then be obtained by designing the PT elements for an effective frame stiffness condition defined below from a frame analysis by the method of virtual work.

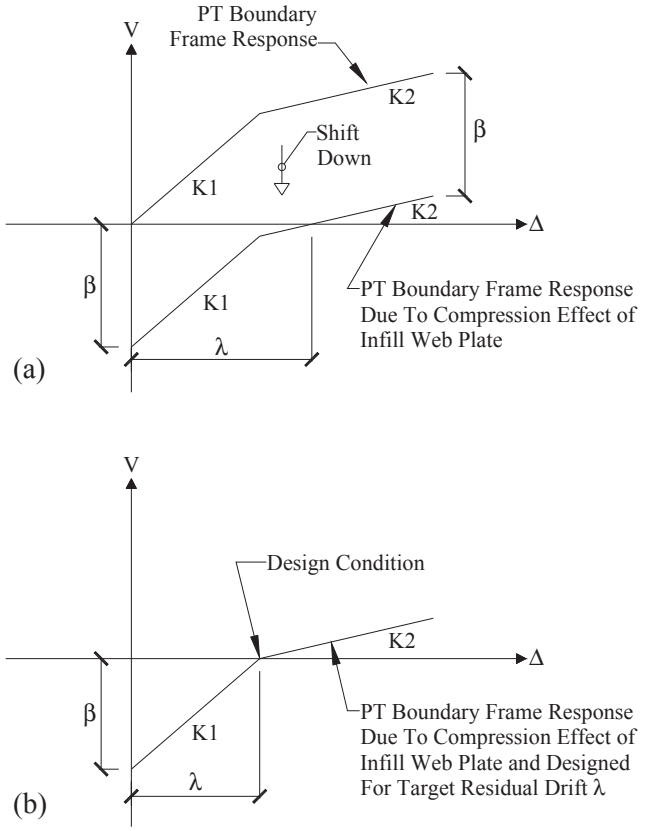

Fig. 16. PT boundary frame response: (a) generic condition; (b) design condition.

$$K_{eff} = \frac{\beta}{\lambda} \tag{3}$$

This can be illustrated by an example using frame NZW. Consider the rightward drift shown in Fig. 17 where: V is the total base shear; h_i is the story heights; W_i is the frame tributary effective seismic weight, C_i is the distribution of base shear along the frame height, θ is the frame drift rotation assumed for a rigid boundary frame, M_{conn} is the strength of the HBE-to-VBE PT rocking joint, P_s is the total PT force in the PT elements at each HBE-to-VBE joint; and y is the distance from the rocking point to the centroid of the PT elements. For simplicity in this example, assuming that the story heights are all equal to h, and floor seismic weights are all equal to W, it then follows from the principle of virtual work and using a plastic analysis approach [28], the external work is:

$$W_E = (C_3V)[\theta(3h)] + (C_2V)[\theta(2h)] + (C_1V)[\theta(h)] \tag{4}$$

and the internal work is,

$$W_I = \sum M_{conn}\theta \tag{5}$$

Next, setting Eq. (4) equal to Eq. (5), then substituting the C_i distribution factors shown in Fig. 17c and solving for V, leads to the approximate strength of the PT boundary frame as:

$$V = \frac{6}{14}\left(\frac{\sum M_{conn}}{h}\right) \tag{6}$$

Furthermore, since the design approach presented here uses an effective global frame stiffness to obtain the approximate area of PT for a given β/λ ratio, the height to the resultant of the total story shear force, H, is required and is determined by equilibrium of the resultant overturning moment of the resultant story forces (i.e., base shear V), equated to the overturning moment due to the story forces such that:

$$(V)(H) = (C_1V)(h) + (C_2V)(2h) + (C_3V)(3h) \tag{7}$$

Substituting the C_i distribution factors shown in Fig. 17c and solving for H leads to:

$$H = \frac{14}{6}h \tag{8}$$

Next, the equation for the effective PT boundary frame strength can be written as shown in Eq. (9), where Δ_{eff} is the lateral displacement at height H indicated by Eq. (8).

$$\begin{aligned} V &= (K_{eff})(\Delta_{eff}) \\ &= (K_{eff})(\theta H) \\ &= (K_{eff})(\theta)\left(\tfrac{14}{6}h\right) \end{aligned} \tag{9}$$

Furthermore, substituting Eq. (6) for V into Eq. (9), then solving for K_{eff} leads to:

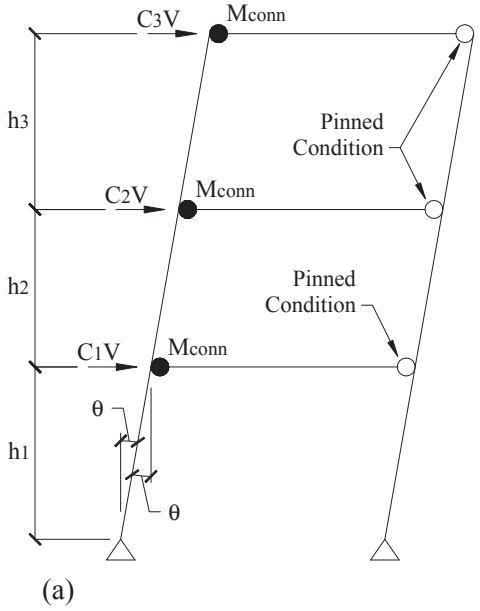

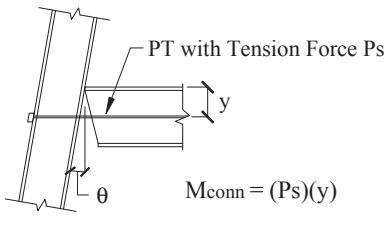

Level	hi	Wi	hiWi	$C_i = \frac{h_iW_i}{\Sigma h_iW_i}$
3	3h	W	3hW	1/2
2	2h	W	2hW	1/3
1	1h	W	1hW	1/6
			Σ = 6hW	Σ = 1

(c)

Fig. 17. Frame NZW post-tension design example: (a) rigid frame sway mechanism; (b) joint moment strength; (c) frame lateral force distribution.

$$K_{eff} = \left(\frac{6}{14h}\right)^2 \left(\frac{\sum M_{conn}}{\theta}\right) \tag{10}$$

In Eq. (10), M_{conn} is the post-tension force, P_s, multiplied by the moment lever arm y from the rocking point to the centroid of the PT elements, and includes both an initial PT force, P_o, and a drift induced PT force which also considers PT force losses, such that:

$$M_{conn} = \left[P_o + \frac{A_{PT} E_{PT}}{L_{PT}} (\Delta_{drift} - \Delta_{loss})\right](y) \tag{11}$$

where A_{PT}, E_{PT}, and L_{PT} is the area, modulus of elasticity, and length of the PT elements, respectively. Additionally, Δ_{drift} is the drift induced PT elongation and Δ_{loss} is the PT relaxation due to HBE axial shortening [6]. Furthermore, to keep the equations manageable for the purpose of initial calculations, the PT force loss term is neglected in Eq. (11) here (for final design, this effect could be accounted for using a nonlinear pushover analysis). Thus, by substituting Eq. (11) into Eq. (10), replacing the summation term with N_{conn} (i.e., total number of M_{conn} considered in frame strength), and solving for A_{PT} leads to the following:

$$A_{PT} = \left(\frac{K_{eff}}{N_{conn}}\right)\left[\left(\frac{14}{6}\frac{h}{y}\right)^2 \left(\frac{L_{PT}}{E_{PT}}\right)\right] - \left(\frac{P_o}{y}\right)\left(\frac{L_{PT}}{E_{PT}}\right)\left(\frac{1}{\theta}\right) \tag{12}$$

Next, substituting Eq. (3) into Eq. (12) for a target K_{eff}, Eq. (12) can be re-written as follows:

$$A_{PT} = \left(\frac{1}{N_{conn}}\right)\left(\frac{\beta}{\lambda}\right)\left[\left(\frac{14}{6}\frac{h}{y}\right)^2 \left(\frac{L_{PT}}{E_{PT}}\right)\right] - \left(\frac{P_o}{y}\right)\left(\frac{L_{PT}}{E_{PT}}\right)\left(\frac{1}{\theta}\right) \tag{13}$$

Eq. (13) provides the required area of PT, for the case of an axially rigid HBE at an HBE-to-VBE joint, for a target effective stiffness, β/λ, for the lateral force distribution shown in Fig. 17. For frame configurations other than shown, the virtual work calculation in determining the strength of the PT boundary frame, V, would need to be modified accordingly. Additionally, Eq. (13) is "exact" for the condition $P_o = 0$, but this term can conservatively be assumed to be zero for the purpose of an initial calculation. A nonlinear cyclic pushover analysis could be conducted to obtain the approximate value of β, for a frame model considering some compression strength of the infill web plate. Alternatively, an approximation could be obtained from a nonlinear monotonic pushover analysis of a tension-only model by assuming some percentage of the peak base shear value. As presented earlier, the analytical models could consider approximately 10% to 20% of the tensile yield strength of the infill web plate for the compression strength of the infill web plates.

For this example, from a nonlinear cyclic pushover analysis, β was obtained to be approximately 30 kN for the frame NZW considered. Additionally, as shown in Fig. 17a, the condition when full relaxation occurs at the closing joints (i.e., represented by zero-rotational stiffness leading to idealized pinned connections) is assumed (i.e., $N_{conn} = 3$) which corresponds to setting K_{eff} to K2 (shown in Fig. 5). Furthermore, a target residual roof drift of 0.2% is selected, such that λ is equal to $(0.002)(h_{roof} = 3759\,\text{mm}) = 7.5\,\text{mm}$, and P_o is conservatively taken to be zero. Eq. (13) indicates that 1432 mm square of PT is required. The resulting global hysteretic response is shown in Fig. 18, which indicates a residual roof drift of approximately 0.24%, comparable to the target 0.2%; also shown in the figure are the results for the original PT configuration for reference. Furthermore, for illustration purposes, only the area of PT strands was increased in this example and the boundary frame was assumed to remain elastic. Accordingly, the boundary frame member sections would require modification as warranted, commensurate with increased strength demands due to the increase in PT forces.

Note that the design approach presented is based on the observation that for static cyclic loading conditions for progressive increase in roof drifts, frame recentering is affected by the compression effects of a solid infill web plate configuration. As noted earlier, experimental results presented in [26] show that frame recentering is not affected by the infill web plate compression strength for earthquake loadings. Furthermore, Eq. (13) assumes a lateral force distribution based on a first mode shape estimate. Therefore, the influence of higher mode effects is not considered. However, the approach presented assumes that the PT elements at the closing-joint end of the HBEs is assumed to be zero, which may or may not occur with consideration of higher mode effects. Therefore, while this general approach may still be applied, it is expected to lead to an upperbound design condition on the post-tension elements. But this approach could facilitate an initial PT boundary frame design, which could then be refined through nonlinear response history analyses of the designed frame specific for the design earthquake loadings considered.

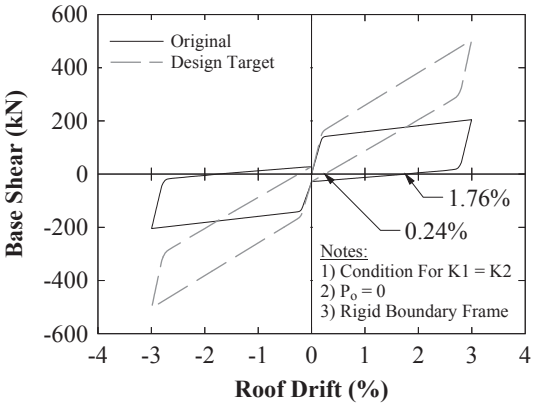

Fig. 18. Frame NZW post-tension design example results.

11. Summary and conclusions

Experimental results from a quasi-static testing program were presented for a recently proposed Self-Centering Steel Plate Shear Wall (SC-SPSW) with three different HBE-to-VBE rocking joint connections and two infill web plate configurations. It was shown that for a multiple actuator configuration along the height of a multi-story SPSW specimen, a top level displacement control with force control of the lower actuators is necessary to avoid undesired actuator interaction along the frame heights. This actuator loading control was used to investigate SC-SPSWs having HBE-to-VBE PT rocking connections that: (i) rock about the HBE top flanges (frame NZ), and (ii) a HBE centerline rocking connection (frame CR). The significance of these connections is that they eliminate beam-growth, that occurs with rocking connections about the top and bottom HBE flanges (frame FR).

From the base shear versus roof drift response, it was found that solid infill web plates provide some additional strength and energy dissipation due to their strength in compression. This is due to the random folding of the infill web plate under cycles of progressively increasing frame drift as a consequence of plastic contraction of the web plate in the direction perpendicular of the web plate tension field. Although this affected frame recentering for quasi-static cyclic loading conditions for progressive roof drift loadings, it has been reported elsewhere that it is not significant under dynamic earthquake excitations. By comparison, frames with infill web strips were shown to respond as tension-only elements under quasi-static cyclic loading. Accordingly, recentering is achieved without the need to consider any compression strength effects of the infill web strips. Of particular significance, frames with infill web strips were cyclically loaded upwards to 9% roof drift where no tearing of the infill web strips from the boundary frame occurred. Compared to frames with solid infill web plates, tearing from the boundary frame initiated at approximately 2% roof drift with significant subsequent tearing. Therefore, infill web strip configurations could be an alternative to solid infill web plate configurations to eliminate tearing from the boundary frame. The use of infill

web strips would also facilitate infill web strip replacement after a design level earthquake compared to replacement of solid infill web plates.

Numerical modeling and results using the program OpenSees was presented. From calibration with the experimental results, compression strength of approximately 20% and 10% of the yield strength of the SPSWs were determined for use in the numerical models for solid infill web plates and strips, respectively. However, given that the infill web strips were shown to be tension-only systems, this suggests that the actual compression strength of the solid infill web plate in these experiments was approximately 10%. Specifically, the simple shear plate connections of the HBEs-to-VBEs and diaphragm connections in the test setup contributed to approximately 10% of the global strength of the PT boundary frame. Furthermore, analytical equations describing the PT response were provided and shown to provide an upperbound prediction to the experimental results. Finally, to also facilitate initial PT design for frames with solid infill web plates, a simple design approach was presented for the calculation of the HBE PT needed to limit the residual roof drift to a target value under quasi-static cyclic loading conditions. The results presented provide insight on the response of post-tensioned steel frames with HBE-to-VBE rocking connections that eliminate beam-growth. The combined contribution of the elastic response of the PT boundary frame with the inelastic response of the replaceable infill web plates, show that SC-SPSWs can be an effective Seismic-Force Resisting System.

Acknowledgements

Financial support for this study was provided by the National Science Foundation as part of the George E. Brown Network for Earthquake Engineering Simulation under award number CMMI-0830294. Additional financial support for D. Dowden was provided by MCEER. Any opinions, findings, conclusions, and recommendations presented in this paper are those of the authors and do not necessarily reflect the views of the sponsors.

References

[1] Dowden DM, Purba R, Bruneau M. Behavior of self-centering steel plate shear walls and design considerations. J Struct Eng, ASCE 2012;138(1):11–21.
[2] Clayton PM, Berman JW, Lowes LN. Seismic design and performance of self-centering steel plate shear walls. J Struct Eng, ASCE 2012;138(1):22–30.
[3] Sabelli R, Bruneau M. Steel Plate Shear Walls. AISC Steel Design Guide 20. Chicago, Ill: American Institute of Steel Construction, Inc.; 2007.
[4] Driver RG, Kulak GL, Kennedy DJL, Elwi AE. Seismic behavior of steel plate shear walls. Structural Engineering Report 215. Edmonton, Alberta, Canada: Department of Civil Engineering, University of Alberta; 1997.
[5] Qu B, Bruneau M, Lin CH, Tsai KC. Testing of full scale two-story steel plate shear walls with reduced beam section connections and composite floors. J Struct Eng, ASCE 2008;134(3):364–73.
[6] Dowden DM, Bruneau M. Analytical and experimental investigation of self-centering steel plate shear walls. Tech. Rep. MCEER-14-0010. Buffalo, New York: Multidisciplinary Center for Earthquake Engineering Research, State University of New York Buffalo; 2014.
[7] Dowden DM, Clayton PM, Li C-H, Berman JW, Bruneau M, Lowes LN, et al. Full-scale pseudo-dynamic testing of self-centering steel plate shear walls. J Struct Eng, ASCE 2016. https://doi.org/10.1061/(ASCE)ST.1943-41X.0001367.
[8] Clayton PM. Self-centering Steel Plate Shear Wall: Subassembly and Full-scale Testing PhD. dissertation Seattle, WA: Dept. of Civil and Environmental Engineering, University of Washington; 2013.
[9] Dowden DM, Bruneau M. Kinematics of self-centering steel plate shear walls with NewZ-BREAKSS post-tensioned rocking connection. Engineering J, AISC, Third Quarter; 2016. p. 117–35.
[10] Cheok G, Stone WC. Performance of 1/3-scale model precast concrete beam-column connections subjected to cyclic inelastic loads – Report No. 4. NISTIR 5436. Gaithersburg, MD: National Institute of Standards and Technology, NIST, June.
[11] MacRae GA, Priestley MJN. Precast post-tensioned ungrouted concrete beam-column subassemblage tests. Structural System Research Report, SSRP 94/10. La Jolla, CA: University of California at San Diego; 1994. 124 pp.
[12] Ricles JM, Sause R, Peng S, Lu L. Experimental evaluation of earthquake resistant posttensioned steel connections. J Struct Eng, ASCE 2002;128(7):850–9.
[13] Christopoulos C, Filiatrault A, Uang CM, Folz B. Posttensioned energy dissipating connections for moment-resisting steel frame. J Struct Eng, ASCE 2002;128(9):1111–20.
[14] Garlock M, Ricles J, Sause R. Experimental studies of full-scale posttensioned steel connections. J Struct Eng, ASCE 2005;131(3):438–48.
[15] Rojas P, Ricles JM, Sause R. Seismic performance of post-tensioned steel moment resisting frames with friction devices. J Struct Eng, ASCE 2005;131(4):529–40.
[16] FEMA State of the Art Report on Systems Performance of Steel Moment Frames Subject to Earthquake Ground Shaking. Rep. No. 355c, SAC Joint Venture for the Federal Emergency Management Agency, Washington, D.C.; 2000.
[17] Purba R, Bruneau M. Seismic performance of steel plate shear walls considering various design approaches. Tech. Rep. MCEER-14-0005. Buffalo, New York: Multidisciplinary Center for Earthquake Engineering Research, State University of New York Buffalo; 2014.
[18] ASCE Minimum Design Loads for Buildings and Other Structures. ASCE/SEI 7-10. Reston, VA: American Society of Civil Engineers; 2010.
[19] AISC Seismic Provisions for Structural Steel Buildings, ANSI/AISC 341-10. Chicago, IL: American Institute of Steel Construction; 2010.
[20] Mazzoni S, McKenna F, Scott MH, Fenves GL. Open system for earthquake engineering simulation user command-language manual – OpenSees version 2.0, Pacific Earthquake Engineering. Berkeley, CA: Research Center, University of California Berkeley; 2009.
[21] Kusumastuti D. A Versatile Experimentation Model for Study of Structures Near Collapse: Applications to Seismic Evaluation of Irregular Structures PhD dissertation Buffalo, NY: Dept of Civil and Environmental Engineering, University at Buffalo; 2005.
[22] ATC Guidelines for Seismic Testing of Components of Steel Structures. Applied Technology Council, Report 24; 1992.
[23] Winkley TB. Self-centering Steel Plate Shear Walls: Large Scale Experimental Investigation MS. thesis Seattle, WA.: Dept. of Civil and Environmental Engineering, University of Washington; 2011.
[24] Webster DJ. The behavior of un-stiffened steel plate shear wall web plates and their impact on the vertical boundary elements PhD dissertation Seattle, WA: Dept of Civil and Environmental Engineering, University of Washington; 2013.
[25] FEMA. Prestandard and Commentary for the Seismic Rehabilitation of Buildings, FEMA 356, prepared by the American Society of Civil Engineers for the Federal Emergency Management Agency, Washington D.C.; 2000.
[26] Dowden DM, Bruneau M. Dynamic shake-table testing and analytical investigation of self-centering steel plate shear walls. J Struct Eng, ASCE 2016. https://doi.org/10.1061/(ASCE)ST.1943-541X.0001547.
[27] Garlock M, Li J. Steel self-centering moment frames with collector beam floor diaphragms. J Constr Steel Res 2008;64(5):526–38.
[28] Berman JW, Bruneau M. Plastic analysis and design of steel plate shear walls. J Struct Eng, ASCE 2003;129(11):1448–56.